Phase diagram of oxygen at extreme pressure and temperature conditions: An *ab initio* study

Beatriz H. Cogollo-Olivo
Universidad de Cartagena, Doctorado en Ciencias Físicas Cartagena de Indias, 130001, Colombia and The Abdus Salam ICTP, Condensed Matter and Statistical Physics Section Trieste, Strada Costiera 11, 34151, Italy

Sananda Biswas
The Abdus Salam ICTP, Condensed Matter and Statistical Physics Section Trieste, Strada Costiera 11, 34151, Italy and Institut für Theoretische Physik, Goethe-Universität Frankfurt, 60438 Frankfurt am Main, Germany

Sandro Scandolo
The Abdus Salam ICTP, Condensed Matter and Statistical Physics Section Trieste, Strada Costiera 11, 34151, Italy

Javier A. Montoya
Universidad de Cartagena, Instituto de Matemáticas Aplicadas Cartagena de Indias, 130001, Colombia

(Received 4 May 2018; revised manuscript received 21 July 2018; published 6 September 2018)

The phase diagram of solid oxygen at terapascal pressures and several thousand Kelvin has been studied with *ab initio* density functional theory within the quasiharmonic approximation for the vibrational free energy. Our work extends previous theoretical studies done at zero temperature and shows that temperature has a dramatic effect on the sequence of phases. At low temperature, the transition from onefold (molecular) to fourfold coordination takes place through two intermediate phases with twofold coordination and space groups $I4_1/acd$ and $Cmcm$. Above 8000 K we find that these two intermediate phases are no longer stable, and oxygen transforms directly from a molecular phase to a fourfold coordinated phase of space group $Fmmm$. We also find that the transition between $Cmcm$ and $Fmmm$ can be ascribed as a second-order transition driven by an electronic instability.

DOI: 10.1103/PhysRevB.98.094103

I. INTRODUCTION

Owing to the magnetic character of the O_2 molecule, the element oxygen exhibits a richer phase diagram than other low-Z diatomic molecules such as H_2, N_2, CO, or F_2. Six phases of solid oxygen have been observed experimentally so far: Half of them (α, β, and γ) exist under equilibrium vapor pressure, and the other three (δ, ϵ, and ζ) are obtained in the high-pressure regime. As pressure increases, oxygen shows a wide range of physical properties that go from insulating [1] to metallic [2], including also antiferromagnetic [3–6] and superconducting [7,8] phases. At the highest pressure reached for this element in the laboratory, about 130 GPa under diamond-anvil cell compression, it remains molecular [8]. In the ϵ-O_2 phase, which is stable between 8 and 96 GPa at ambient temperature [2], the oxygen molecules associate into clusters composed of four molecules, but they fully retain their molecular character as confirmed by vibrational spectroscopy and x-ray diffraction [9,10].

All other group-VI elements develop nonmolecular and eventually monoatomic structures at much lower pressure. Sulfur transforms into a chainlike polymeric phase at about 15 GPa and eventually becomes monoatomic, with a rhombohedral β-Po structure at 153 GPa [11]. Phases with a β-Po structure are also reported for Se at 60 GPa [12], for Te at 11 GPa [13], and for Po at ambient pressure [14]. Moreover, both selenium and tellurium exhibit a body-centered cubic (bcc) structure as a post β-Po phase [12,15,16]. For oxygen, however, an earlier theoretical study has shown that the monoatomic β-Po structure is less stable than molecular phases at multimegabar pressures [17]. The reluctance of oxygen to give up its molecular character has been attributed in a recent study by Sun *et al.* to the strong electron lone-pair repulsion in the nonmolecular phases. This resembles, we notice, the reluctance of the electron-richer halogen elements to lose their molecular character. For instance, fluorine is molecular up to the highest pressures experimentally achieved so far in this element [18], while Cl_2, Br_2, and I_2 dissociate around 157, 115, and 43 GPa, respectively [19–27].

In the same work, Sun *et al.* [28] show that oxygen remains molecular up to 1.9 TPa before transforming into a semiconducting square-spiral-like polymeric structure with symmetry $I4_1/acd$ and oxygen in twofold coordination. This phase is then reported to transform at 3.0 TPa into a phase with $Cmcm$ symmetry, consisting of zigzag chains that pack atoms more efficiently than the square-spiral chains. Finally, when pressure reaches 9.3 TPa, the in-plane zigzag chains merge into a layered structure with $Fmmm$ symmetry and four equidistant nearest neighbors for each oxygen atom [28].

Temperature can have profound effects on the stability of molecular phases, both in their liquid and solid forms. Shock-compression experiments indicate that at about 100 GPa the oxygen molecule dissociates in the fluid when the temperature exceeds 4000 K [29], whereas theoretical studies based on

ab initio molecular dynamics place molecular dissociation above 80 GPa at temperatures that exceed 5000 K [30]. Unfortunately, nothing is known about the temperature effects on the phase diagram of *solid* oxygen at extreme pressures. A crude extrapolation of the oxygen melting line, based on theoretical and experimental data [31,32], yields a melting temperature of about 26 000 K at 1.9 TPa. Although this extrapolation is based on data below 100 GPa and is, therefore, to be taken with caution, this provides a hint that solid oxygen phases could indeed be the stable forms of this element in some planetary interiors. Hence, the understanding of the effects of temperature on the solid portion of oxygen's phase diagram at multimegabar pressures is not only relevant from a fundamental perspective, but also for its potential relevance to planetary studies. Moreover, recent technical developments in dynamic shock-wave (ramp) compression have made it possible to achieve temperature and pressure conditions in the laboratory that are within the solid portion of selected phase diagrams [33–35], suggesting that experiments may soon be able to study the properties of this element at planetary conditions.

The ground state calculations performed by Sun *et al.* [28] show that the transitions from molecular to polymeric and finally to fourfold coordinated have dramatic effects on the vibrational properties of solid oxygen. Finite-temperature contributions to the free energy should, therefore, differ substantially between different phases and the phase transitions at high temperature may, as a consequence, differ quantitatively and qualitatively from the ones calculated at zero temperature. In this work, by performing density functional theory (DFT) together with quasiharmonic approximation (QHA) calculations for the determination of vibrational free energies, we extend the current theoretical knowledge on the ultrahigh-pressure region of the phase diagram of solid oxygen to temperatures up to 8000 K. We find that temperature has a remarkable effect on the phase diagram of this element indeed, resulting in the disappearance of two previously reported nonmolecular forms at sufficiently high temperature.

II. METHODS

Out of the several crystalline structures considered in the earlier theoretical work by Sun *et al.* [28], we select here the ones that were found to be stable in the range of pressure 1–10 TPa: a molecular structure with symmetry $R\bar{3}m$ and three nonmolecular structures with symmetry $I4_1/acd$, $Cmcm$, and $Fmmm$, respectively. Enthalpy differences among the different molecular structures considered in Ref. [28] ($P6_3/mmc$, $C2/m$, $C2/c$, and $R\bar{3}m$) are small compared to enthalpy differences between molecular and nonmolecular structures, so we expect transition pressures between molecular and nonmolecular phases to be largely independent of the specific molecular structure considered. Here we consider the $R\bar{3}m$ phase as representative of the stable solid molecular oxygen form before polymerization and tested the validity of this assumption with a test calculation on a different molecular structure with symmetry $C2/m$.

The structural properties were calculated using DFT as implemented in QUANTUM ESPRESSO [36]. The electron-ion interactions were treated using a projector augmented wave pseudopotential with six valence electrons. The valence electron wave functions are expanded in a plane-wave basis set with a kinetic energy cutoff of 400 Ry. The exchange-correlation functional was approximated by the generalized gradient approximation (GGA) of the Perdew-Burke-Ernzerhof form [37]. Brillouin zone integrations were carried out using k-point grids generated with the Monkhorst-Pack method [38]. The size of these grids are $18 \times 18 \times 18$, $4 \times 4 \times 12$, $8 \times 16 \times 16$, and $8 \times 16 \times 16$ for the primitive cells of the four phases of oxygen considered in this study; these choices provided a total-energy-difference convergence of 2 meV per atom or better. The structural parameters for all the structures were obtained by performing variable cell optimization at various values of pressure. Note that the energies and electronic structures of the four structures have been already studied by Sun *et al.* [28]; they showed that at $T = 0$ K, all the phases are metallic at the terapascal regime, except for $I4_1/acd$ which is a wide-gap semiconductor. Our calculations agree well with those results, as discussed in Sec. III. For the metallic phases, the calculations were done using the Fermi-Dirac smearing technique with a width of 43 meV, in order to take into account the electronic entropy at 500 K. This width was kept fixed while calculating the vibrational properties at all temperatures, as justified by the lack of sensitivity of our free energy results with respect to this parameter.

The vibrational properties at $T = 0$ K were calculated using density functional perturbation theory (DFPT) in the linear response regime [39]. The q-point grids used to obtain the dynamical matrices were as follows: $4 \times 4 \times 4$ for $R\bar{3}m$, $2 \times 2 \times 6$ for $I4_1/acd$, $2 \times 4 \times 4$ for $Cmcm$, and $2 \times 4 \times 4$ for $Fmmm$.

Finite-temperature contributions to the Helmholtz free energy were obtained using the QHA [40,41]:

$$F(V,T) = U_0(V) + \frac{1}{2}\sum_{\mathbf{qs}} \hbar\omega_{\mathbf{qs}} + k_B T \sum_{\mathbf{qs}} \ln[1 - \exp(-\hbar\omega_{\mathbf{qs}}/k_B T)], \quad (1)$$

where $\omega_{\mathbf{qs}}$ is the frequency of the mode $\mathbf{s}$ at point $\mathbf{q}$ in the Brillouin zone and a given volume V; $U_0(V)$ is the ground state electronic energy of the crystal at volume V, and the second and third terms on the right-hand-side of the above equation are the zero-point energy (ZPE) and the thermal vibrational contribution to the free energy, respectively, at volume V.

As we are interested in determining the pressure-temperature (P-T) phase diagram, we have calculated the Gibbs free energy as:

$$G(P,T) = F[V(P,T),T] + PV(P,T), \quad (2)$$

where the value of the P is obtained by fitting Eq. (1) to a third order Birch-Murnaghan equation of state for each of the phases at different temperatures and their corresponding parameters are specified in the Supplemental Material [42]. All fits had a variance (χ^2) of order 10^{-5} or better.

III. RESULTS AND DISCUSSION

We begin our analysis by considering the case $T = 0$ K, with and without the zero-point energy contributions. In the

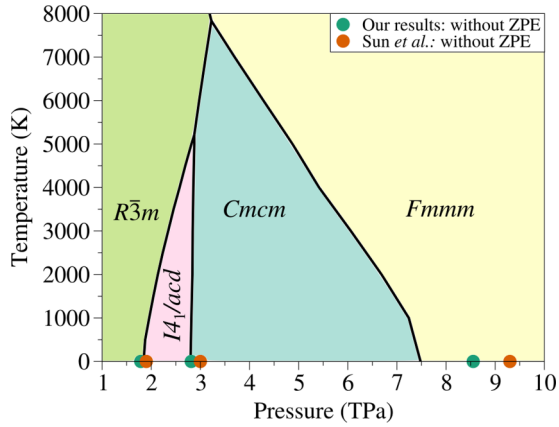

FIG. 1. Proposed finite temperature phase diagram for solid oxygen at extreme conditions of pressure and temperature. The transition pressures P_T, at zero temperature without taking into account the zero-point energy (ZPE), reported by Sun *et al.* [28] and calculated in the present study, are marked as orange and green circles, respectively. The phase boundaries at finite temperature, corresponding to calculations including ZPE and using an electronic temperature of 500 K, are shown by solid black lines.

low-pressure region of this study we find that the contribution of the ZPE is marginal, moving the transition pressures 0.08 TPa and 0.02 TPa higher than those reported without ZPE when going from $R\bar{3}m$ to $I4_1/acd$ and from $I4_1/acd$ to $Cmcm$, respectively (see Fig. 1). In the high-pressure region, our enthalpy-pressure relations show that the transition from $Cmcm$ to $Fmmm$ at 0 K is located near 8.6 TPa if ZPE is not included; this is 0.7 TPa lower than the transition pressure found by Sun *et al.* with the same approximations [28]. Our equations of state were fitted on a broader set of volumes than Sun *et al.*, usually fifteen or more volumes per structure. We believe that this could be one of the reasons for the discrepancy. Moreover, when the ZPE contribution is included, it has a noticeable effect, shifting the transition pressure from 8.6 TPa to 7.5 TPa.

We now consider the effects of finite temperature on the Gibbs free energies and transition pressures. Our calculations are based on the QHA and may suffer from the incomplete consideration of anharmonicities, in particular when the system approaches the melting temperature, therefore, our analysis is restricted here to temperatures below 8000 K.

The finite temperature contribution to the free energy has dramatic consequences on the relative stability of the crystalline phases (Fig. 1). For instance, the pressure location for the $R\bar{3}m$ to $I4_1/acd$ phase boundary is shifted towards higher pressures by approximately 1 TPa when the temperature is raised from 0 to 5000 K, indicating that the molecular $R\bar{3}m$ phase enlarges its region of stability with respect to the polymeric $I4_1/acd$, as temperature increases. However, the finite temperature contribution hardly changes the transition boundary between the phases $I4_1/acd$ and $Cmcm$, as we observed an increment of just 0.05 TPa at 5000 K with respect to the transition pressure calculated at 0 K. We observe that the region that encompassed the $I4_1/acd$ phase narrows down as temperature increases until, at 2.9 TPa and 5200 K, there is a triple point above which this phase disappears completely. Thus, the picture of $I4_1/acd$ as an insulating solid phase lying between two metallic ones ($R\bar{3}m$ and $Cmcm$) is only valid at relatively low temperatures. Unlike the previous two cases, the shift seen in the case of the $Cmcm$-to-$Fmmm$ transition is towards lower pressures and is much more pronounced, leading to a second triple point at 3.2 TPa and 7800 K, where the $R\bar{3}m$, $Cmcm$, and $Fmmm$ phases meet. This indicates that above 8000 K oxygen transforms directly from a molecular to a fourfold coordinated form.

So far our analysis has been restricted to a single molecular structure ($R\bar{3}m$). In order to test the validity of our assumption that $R\bar{3}m$ can be considered as representative of the stable molecular structure, we repeated the calculations with a different molecular structure, of symmetry $C2/m$. This structure was found to possess the second lowest enthalpy after $R\bar{3}m$, among the structures considered by Sun *et al.* [28]. We find that the transition line between $C2/m$ and the other structures is indistinguishable from the transition line of $R\bar{3}m$, suggesting that not only enthalpy but also entropy is very similar among different molecular forms.

As already mentioned, an extrapolation of the measured melting line of oxygen to TPa pressures yields a melting temperature exceeding 25 000 K at 2 TPa. An independent estimate of the melting temperature can be obtained by calculating the Lindemann ratio of the solid phases, a quantity that normally reaches values between 0.1 and 0.15 at melting. We calculated the Lindemann ratio for the $R\bar{3}m$ molecular structure and for the $Fmmm$ structure within the QHA approximation. In the case of the molecular structure we

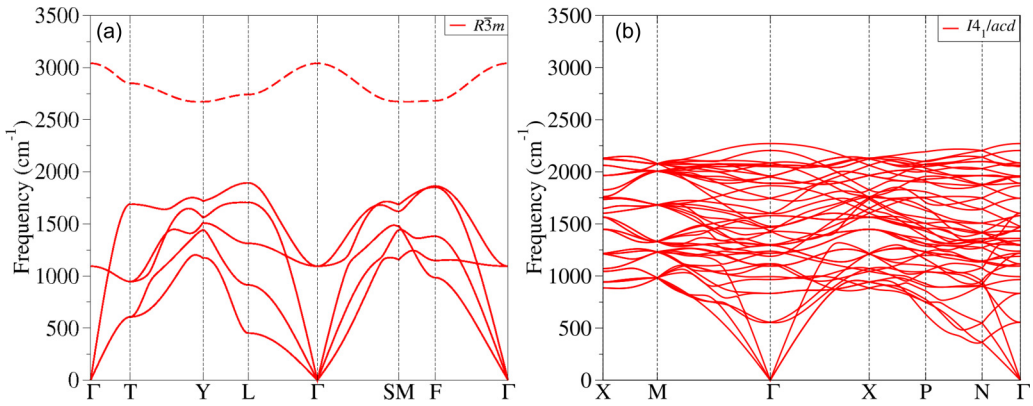

FIG. 2. Phonon dispersions of oxygen in (a) $R\bar{3}m$ with the vibron mode in dashed line and (b) $I4_1/acd$ phases at 2.0 TPa.

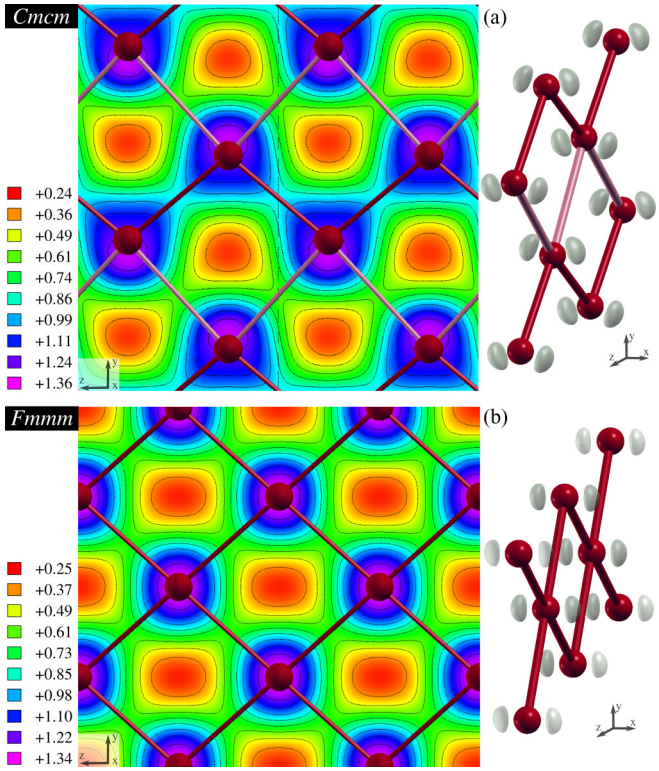

FIG. 3. Electronic charge densities along the [100] direction and electron lone pairs of (a) $Cmcm$ and (b) $Fmmm$ at 7.5 TPa. The color scales indicate the values of the charge density in e/Bohr^3. On the left panel, the isosurface of red and orange regions are electron poor, while blue and violet regions are electron rich. Additionally, isosurface contours are shown by solid black lines. On the right panel, the lone pairs are represented by transparent gray colors; the corresponding isosurface value is $+1.25\ e$/Bohr^3. The oxygen atoms are represented by red spheres and the $Cmcm$ zigzag chains are shown in red and pink.

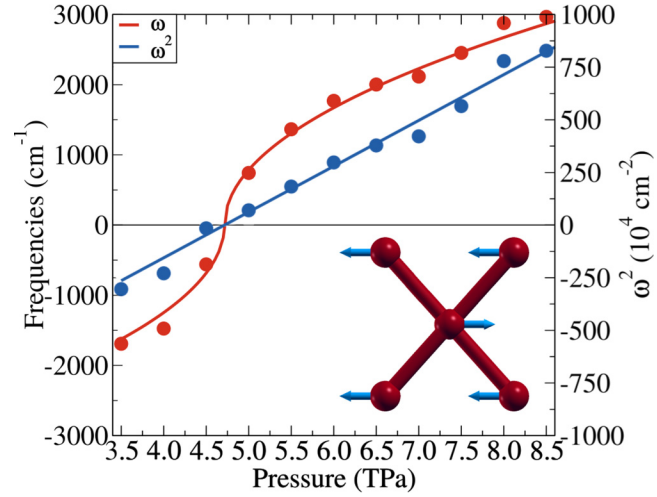

FIG. 5. Evolution of a $Fmmm$ phonon mode at the zone boundary as a function of pressure. The normal mode is along the [100] direction, and its frequencies (ω) are plotted in red. A linear relation between the squared phonon frequencies (ω^2) and pressure (blue) is observed and indicates that the phonon softening occurs near 4.7 TPa. The normal mode is represented as blue arrows on the atoms of the $Fmmm$ structure.

assumed that melting takes place between a molecular solid and a molecular liquid and evaluated the Lindemann ratio based on the mean-square displacement of the center of mass of the molecules. We found that calculated values of L_R are always below 0.095, for both phases, in the temperature range from 0 K to 8000 K. Our calculations therefore rule out the presence of a liquid in the pressure and temperature region considered in this work.

We were also able to confirm that strongly localized lone pairs persist into the polymeric phases with an OX_2E_2 bent shape, as already noted by Sun *et al.* [28]. This, together with an electron counting argument, can explain the reluctance of oxygen to take higher coordinated structures. The formation in $I4_1/acd$ of one additional covalent bond and the lone pair repulsion between chains, contribute to making it stiffer and less flexible than the molecular $R\bar{3}m$ phase. At temperatures below 4000 K the contribution to the entropy of the high frequency vibron in Fig. 2(a) is limited by quantum effects. The remaining modes show a frequency increase across the transition, which implies a decrease of the vibrational entropy. This is consistent with the positive slope of the transition line at finite temperature (see Fig. 1). Similarly, the $I4_1/acd$ and $Cmcm$ phases are characterized by having two covalent bonds per oxygen and very similar lone pair repulsion between

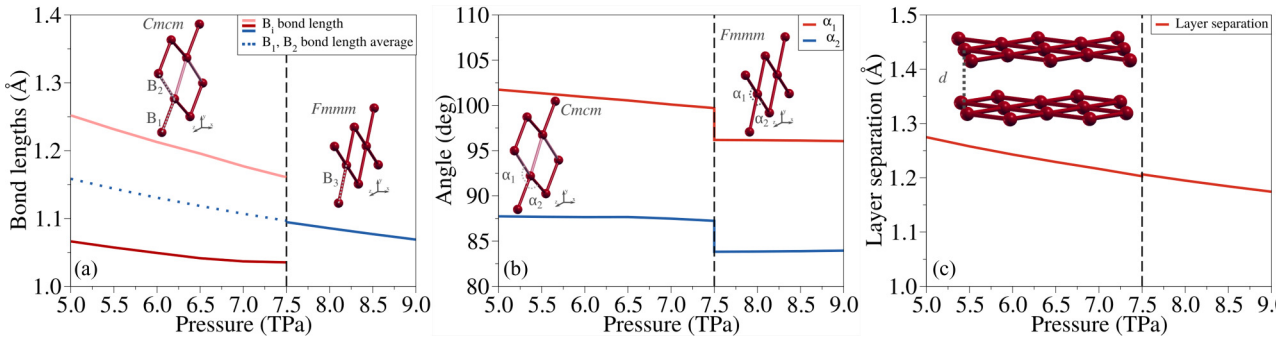

FIG. 4. Pressure dependence of (a) bond lengths for $Cmcm$ (B_1 and B_2, red and pink solid lines, respectively) and $Fmmm$ (B_3, blue solid line), (b) internal angles (α_1 and α_2, red and blue solid lines, respectively) of $Cmcm$ and $Fmmm$, and (c) the layer separation d (red solid line) for $Cmcm$ and $Fmmm$ are shown. The vertical black dashed line corresponds to the calculated transition pressure between these two phases. The average of B_1 and B_2 are also shown by a dotted blue line in (a).

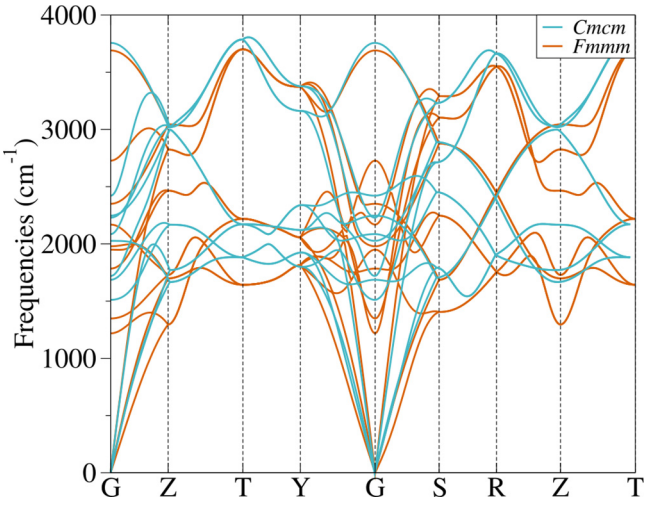

FIG. 6. Phonon dispersions of oxygen in *Cmcm* (in cyan) and *Fmmm* (in orange) phases at 8.0 TPa. Note that the supercell size has been used in both the cases.

chains. Therefore, one does not expect important changes in terms of bonding and stiffness, which justifies why we observe an almost vertical transition line between these two polymeric forms in the P-T phase diagram (Fig. 1).

As pressure increases above 4 TPa and keeps approaching the vicinity of the $Cmcm \rightarrow Fmmm$ transition, the bent shape of the lone pairs in *Cmcm* starts to allow for a nonsymmetrical fourfold coordination, which brings the formation of two additional weak covalent bonds per each oxygen prior to the final transition towards the fully symmetric *Fmmm* configuration; this is shown in Fig. 3(a) by the charge density profiles. This process causes a gradual merging of the so-called zigzag chains into a layered structure. For instance, at $T = 0$ K and 7.0 TPa, the four shortest links for each oxygen consist of two sets of bonds with lengths 1.04 Å and 1.18 Å, respectively. Instead, when *Cmcm* transforms into *Fmmm* above 7.5 TPa not only the coordination of the oxygen atoms becomes symmetrical, with an equal length of 1.10 Å, but also we can see now that the lone pairs adopt the OX_4E_2 square planar shape, as a consequence of the higher symmetry of this phase as Fig. 3(b) shows.

From a space-group point of view, *Cmcm* is a subgroup of *Fmmm* so that the transition can be classified in principle as a second-order phase transition. Coupling of the strain with the internal degrees of freedom, however, introduces a slight discontinuity in the structural parameters (see Fig. 4), similarly to the case of the stishovite (rutile) to the $CaCl_2$-type phase transition in SiO_2 [43]. Further evidence for the quasi-second-order nature of the transition comes from the phonon dispersions of the two phases. In Fig. 5 we show the pressure dependence of the frequency of the phonon mode at the Brillouin zone vector of the *Fmmm* phase corresponding to the reciprocal lattice vector of the *Cmcm* phase. The mode becomes unstable when pressure is decreased below 4.7 TPa, indicating a lattice instability of the *Fmmm* phase towards *Cmcm*, as also confirmed by the pattern of the unstable mode, shown in the inset of Fig. 5. A characteristic feature of second-order phase transitions is the higher entropy of the high-symmetry phase with respect to the low-symmetry phase. This is consistent with the pronounced left turning of the *Cmcm* to *Fmmm* phase transition line at finite temperatures in Fig. 1, and it is confirmed by the phonon dispersions of the two phases calculated at the transition pressure of 8.0 TPa (Fig. 6). Contrary to the naive expectation that frequencies become stiffer in the high-pressure (*Fmmm*) phase with respect to the low-pressure (*Cmcm*) phase, the phonon dispersion of the *Cmcm* phase has modes that are marginally higher in energy than those of the *Fmmm* phase. This is consistent with the lower entropy of the *Cmcm* phase with respect to the *Fmmm* phase.

To gain further insight into the driving force of the quasi-second-order transition, we show in Fig. 7 the electronic density of states (DOS) of the two phases in the vicinity of the pressure where *Fmmm* becomes unstable. Interestingly, the DOS of the *Fmmm* phase shows a pronounced peak that crosses the Fermi level between 4.5 and 5 TPa, the same pressure of the phonon instability reported in Fig. 5. The distortion leading to the *Cmcm* structure causes a lowering of the DOS at the Fermi level. We, therefore, argue that the *Cmcm* to *Fmmm* transition is driven by an electronic

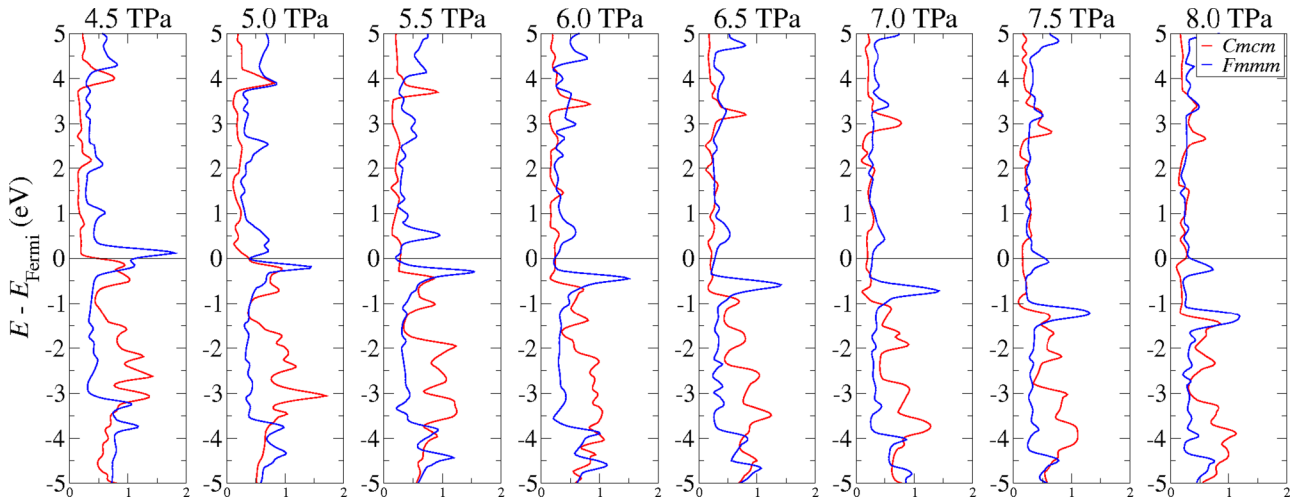

FIG. 7. Electronic DOS of oxygen in *Cmcm* (in red) and *Fmmm* (in blue) phases as a function of pressure.

instability qualitatively similar to a commensurate charge-density-wave transition. A similar phenomenology has been observed in other chalcogen elements, where it has been shown to be connected with the emergence of a superconducting state in the undistorted state ($Fmmm$ in this case) close to the transition pressure to the distorted phase [11].

IV. CONCLUSIONS

Our theoretically predicted phase diagram of oxygen at extreme pressures and temperatures extends earlier calculation at high pressure and zero temperature and shows that temperature has a profound effect on the phase diagram. At finite temperatures, the molecular phase expands its stability range to pressures exceeding 3 TPa at the highest temperatures considered in this work (8000 K). On the contrary, the range of stability of the first nonmolecular phase, $I4_1/acd$, shrinks with temperature and the phase is no longer thermodynamically stable above 5000 K. Interesting physics underlies the transition between the $Cmcm$ and the $Fmmm$ nonmolecular phases. Our calculations indicate a quasi-second-order transition between the two phases and show that the transition is driven by an electronic instability causing a softening of the corresponding phonon mode. We argue that this may imply a superconducting state which is beyond the scope of this work but which certainly deserves further attention. The range of pressures and temperatures examined in this work are now within reach of ramp-compression experiments which we hope will soon shed additional light on the intriguing aspects of the pressure-induced demise of molecular oxygen as reported in this and other recent theoretical studies.

ACKNOWLEDGMENTS

B.H.C.-O. thanks COLCIENCIAS for a graduate scholarship, also the support from the STEP programme of the Abdus Salam International Centre of Theoretical Physics is gratefully acknowledged. J.A.M. thanks the Vicerrectoría de Investigaciones of the Universidad de Cartagena and COLCIENCIAS, for supporting the Grupo de Modelado Computacional (COL0101016).

[1] Y. Crespo, M. Fabrizio, S. Scandolo, and E. Tosatti, Proc. Natl. Acad. Sci. USA **111**, 10427 (2014).
[2] Y. Akahama, H. Kawamura, D. Häusermann, M. Hanfland, and O. Shimomura, Phys. Rev. Lett. **74**, 4690 (1995).
[3] M. Nicol, K. R. Hirsch, and W. B. Holzapfel, Chem. Phys. Lett. **68**, 49 (1979).
[4] D. Schiferl, D. T. Cromer, L. A. Schwalbe, and R. L. Mills, Acta Crystallogr. Sect. B **39**, 153 (1983).
[5] F. A. Gorelli, M. Santoro, L. Ulivi, and M. Hanfland, Phys. Rev. B **65**, 172106 (2002).
[6] I. N. Goncharenko, O. L. Makarova, and L. Ulivi, Phys. Rev. Lett. **93**, 055502 (2004).
[7] Y. Ma, A. R. Oganov, and C. W. Glass, Phys. Rev. B **76**, 064101 (2007).
[8] G. Weck, S. Desgreniers, P. Loubeyre, and M. Mezouar, Phys. Rev. Lett. **102**, 255503 (2009).
[9] L. F. Lundegaard, G. Weck, M. I. McMahon, S. Desgreniers, and P. Loubeyre, Nature (London) **443**, 201 (2006).
[10] H. Fujihisa, Y. Akahama, H. Kawamura, Y. Ohishi, O. Shimomura, H. Yamawaki, M. Sakashita, Y. Gotoh, S. Takeya, and K. Honda, Phys. Rev. Lett. **97**, 085503 (2006).
[11] O. Degtyareva, E. Gregoryanz, H. K. Mao, and R. J. Hemley, High Pressure Research **25**, 17 (2005).
[12] Y. Akahama, M. Kobayashi, and H. Kawamura, Phys. Rev. B **47**, 20 (1993).
[13] J. C. Jamieson and D. B. McWhan, J. Chem. Phys. **43**, 1149 (1965).
[14] R. J. DeSando and R. C. Lange, J. Inorg. Nucl. Chem. **28**, 1837 (1966).
[15] F. El Haj Hassan, A. Hijazi, M. Zoaeter, and F. Bahsoun, Physica B: Condensed Matter **363**, 82 (2005).
[16] M. Otani and N. Suzuki, Phys. Rev. B **63**, 104516 (2001).
[17] T. Oda, K. Sugimori, H. Nagao, I. Hamada, S. Kagayama, M. Geshi, H. Nagara, K. Kusakabe, and N. Suzuki, J. Phys.: Condens. Matter **19**, 365211 (2007).
[18] Q. Lv, X. Jin, T. Cui, Q. Zhuang, Y. Li, Y. Wang, K. Bao, and X. Meng, Chin. Phys. B **26**, 076103 (2017).
[19] P. Li, G. Gao, and Y. Ma, J. Chem. Phys. **137**, 064502 (2012).
[20] T. Kenichi, S. Kyoko, F. Hiroshi, and O. Mitsuko, Nature (London) **423**, 971 (2003).
[21] T. Kume, T. Hiraoka, Y. Ohya, S. Sasaki, and H. Shimizu, Phys. Rev. Lett. **94**, 065506 (2005).
[22] D. Duan, Y. Liu, Y. Ma, Z. Liu, T. Cui, B. Liu, and G. Zou, Phys. Rev. B **76**, 104113 (2007).
[23] A. Fujii, Y. Hase, K. Ohishi, Y. Fujihisa, H. Hamaya, and N. Onodera, Solid State Commun. **59**, 85 (1986).
[24] Y. Fujii, K. Hase, N. Hamaya, Y. Ohishi, A. Onodera, O. Shimomura, and K. Takemura, Phys. Rev. Lett. **58**, 796 (1987).
[25] R. Reichlin, A. K. McMahan, M. Ross, S. Martin, J. Hu, R. J. Hemley, H. K. Mao, and Y. Wu, Phys. Rev. B **49**, 3725 (1994).
[26] Y. Fujii, K. Hase, Y. Ohishi, H. Fujihisa, N. Hamaya, K. Takemura, O. Shimomura, T. Kikegawa, Y. Amemiya, and T. Matsushita, Phys. Rev. Lett. **63**, 536 (1989).
[27] H. Fujihisa, Y. Fujii, K. Takemura, and O. Shimomura, J. Phys. Chem. Solids **56**, 1439 (1995).
[28] J. Sun, M. Martinez-Canales, D. D. Klug, C. J. Pickard, and R. J. Needs, Phys. Rev. Lett. **108**, 045503 (2012).
[29] M. Bastea, A. C. Mitchell, and W. J. Nellis, Phys. Rev. Lett. **86**, 3108 (2001).
[30] B. Militzer, F. Gygi, and G. Galli, Phys. Rev. Lett. **91**, 265503 (2003).
[31] G. Weck, P. Loubeyre, J. H. Eggert, M. Mezouar, and M. Hanfland, Phys. Rev. B **76**, 054121 (2007).
[32] A. F. Goncharov, N. Subramanian, T. R. Ravindran, M. Somayazulu, V. B. Prakapenka, and R. J. Hemley, J. Chem. Phys. **135**, 84512 (2011).
[33] J. R. Rygg, J. H. Eggert, A. E. Lazicki, F. Coppari, J. A. Hawreliak, D. G. Hicks, R. F. Smith, C. M. Sorce, T. M. Uphaus, B. Yaakobi, and G. W. Collins, Rev. Sci. Instrum. **83** (2012).

[34] R. F. Smith, J. H. Eggert, R. Jeanloz, T. S. Duffy, D. G. Braun, J. R. Patterson, R. E. Rudd, J. Biener, A. E. Lazicki, A. V. Hamza, J. Wang, T. Braun, L. X. Benedict, P. M. Celliers, and G. W. Collins, Nature (London) **511**, 330 (2014).

[35] J. Wang, F. Coppari, R. F. Smith, J. H. Eggert, A. E. Lazicki, D. E. Fratanduono, J. R. Rygg, T. R. Boehly, G. W. Collins, and T. S. Duffy, Phys. Rev. B **94**, 104102 (2016).

[36] P. Giannozzi, S. Baroni, N. Bonini, M. Calandra, R. Car, C. Cavazzoni, D. Ceresoli, G. L. Chiarotti, M. Cococcioni, I. Dabo, A. Dal Corso, S. De Gironcoli, S. Fabris, G. Fratesi, R. Gebauer, U. Gerstmann, C. Gougoussis, A. Kokalj, M. Lazzeri, L. Martin-Samos, N. Marzari, F. Mauri, R. Mazzarello, S. Paolini, A. Pasquarello, L. Paulatto, C. Sbraccia, S. Scandolo, G. Sclauzero, A. P. Seitsonen, A. Smogunov, P. Umari, and R. M. Wentzcovitch, J. Phys.: Condens. Matter **21**, 395502 (2009).

[37] J. P. Perdew, K. Burke, and M. Ernzerhof, Phys. Rev. Lett. **77**, 3865 (1996).

[38] H. J. Monkhorst and J. D. Pack, Phys. Rev. B **13**, 5188 (1976).

[39] S. Baroni, S. De Gironcoli, A. Dal Corso, and P. Giannozzi, Rev. Mod. Phys. **73**, 515 (2001).

[40] G. Leibfried and W. Ludwig, Solid State Phys. **12**, 275 (1961).

[41] S. Baroni, P. Giannozzi, and E. Isaev, Reviews in Mineralogy and Geochemistry **71**, 39 (2010).

[42] See Supplemental Material at http://link.aps.org/supplemental/10.1103/PhysRevB.98.094103 for the parameters of the third order Birch-Murnaghan equation of state.

[43] R. Nomura, K. Hirose, N. Sata, Y. Ohishi, D. Suetsugu, C. Bina, T. Inoue, D. Wiens, and M. Jellinek, Phys. Earth Planet. Inter. **183**, 104 (2010).